

# Noncausal Explicit Model Predictive Control of Wave Energy Converters

Teng Gao, Yao Zhang\* and Tahsin Tezdogan

*T.Gao and T.Tezdogan are with the School of Engineering, University of Southampton, Southampton, SO17 1BJ, United Kingdom*

*Y.Zhang is with the Department of Mechanical Engineering, University College London, London, WC1E 7JE, United Kingdom*

---

## ARTICLE INFO

### Keywords:

Wave Energy Converters  
Optimal Control  
Model Predictive Control  
Robustness  
Wave Prediction

## Abstract

Wave energy is a promising renewable energy source, but its commercial utilisation is low compared to wind and solar energy. This paper proposes an explicit model predictive control (EMPC) strategy to reduce the high computational burden associated with online computation. Realistic wave data collected from the coast of Cornwall, UK, together with realistic single-point absorber parameters, are utilised. The dynamic response of the floating system is controlled, and a disturbance observer and an autoregressive model are designed for wave prediction. This paper aims to identify the most effective strategy to achieve optimal trajectory tracking, rapid prediction, efficient optimisation, and maximum energy capture. The results of numerical simulations show impressive effects of trajectory tracking, wave prediction, and maximum energy capture, with rapid prediction and low computational demand. These results demonstrate the effectiveness of the proposed EMPC method in wave energy converters (WECs).

---

## 1. Introduction

In the coming decades, the world's energy consumption will grow significantly. Fossil fuel resources are depleting, and environmental problems such as global warming, rising sea levels, and extreme weather frequently occur. Therefore, the development of clean energy has become a global challenge and shared goal (Clément et al., 2002). The ocean is the world's largest ecosystem, covering 71% of the Earth's surface and holding abundant energy resources. The energy obtained from ocean waves can reach about 32,000 kWh/year (Faedo et al., 2017). Wave energy is a widely distributed and unbalanced renewable resource with high energy density and the potential for a continuous power supply. Resource-intensive areas are mainly concentrated in mid- and high-latitude waters, such as the west coast of North America, southern Australia, the British Isles, the west coast of Europe, southern Chile, and New Zealand (Drew et al., 2009) (Barstow et al., 2011). Compared with renewable energy sources such as wind and solar energy, wave energy has higher energy density and stability. Furthermore, it has been demonstrated that wave prediction can improve control performance (Falnes and Kurniawan, 2020). The annual power generation potential of ocean tidal, seepage, wave, and thermal energy is 800 TWh, 2,000 TWh, 8,000 to 80,000 TWh, and 10,000 to 87,600 TWh, respectively. The potential far exceeds the annual global electricity demand of about 16,000 TWh (Khan et al., 2017).

As technology advances and costs decrease, marine renewable energy has broad prospects and helps promote optimisation of the global energy structure (Qiu et al., 2019). However, despite its advantages, wave energy faces significant technical challenges in harnessing its potential. The main difficulty in obtaining wave energy is that exploiting the irregular reciprocating motion of the ocean is not as simple as obtaining energy from the wind (Ringwood et al., 2014). Early systems used the natural movement of floats with the waves to achieve passive conversion of wave energy, and a variety of floating wave energy converters (WECs) have been developed for wave energy harvesting (Xu et al., 2019). Active control systems apply external forces to adjust the movement of floats to keep them in sync with the wave frequency. The control strategy based on the combination of Model Predictive Control (MPC) and an active valve control mechanism is simple to operate and has the best performance compared to other control methods (Jusoh et al., 2019). However, realistic waves are not single-frequency; they change over time. To achieve automatic adjustment of the ocean's natural frequency, it is essential to implement advanced dynamic control technology under realistic ocean conditions (Yang et al., 2021).

WECs such as point absorbers, oscillating water columns, and attenuators have been studied and developed (Jariwala et al., 2025). Wave prediction methods such as the Extended Kalman Filter (EKF), artificial neural network, and deterministic sea wave prediction (DSWP) all introduce certain prediction errors (Zhang and Li, 2019). Point absorbers have been widely studied in the field of WEC control and are often used as a benchmark

---

\*Corresponding author

 yao.zhang@uc1.ac.uk (Y. Zhang)

ORCID(s): 0000-0002-3821-371X (Y. Zhang)

problem for wave excitation force estimation. It is smaller than the wavelength and uses the up-and-down motion of the float to capture wave energy from waves that are larger than the physical size of the device itself, making it less likely to be damaged in the harsh marine environments (Zhang et al., 2019) (Faizal et al., 2014). Based on the simple control method (SCM) (Fusco and Ringwood, 2012) (Korde and Ringwood, 2016), practical prediction techniques are improved and used for wave observations to almost accurately and simultaneously predict the hydrodynamic forces on the WECs at all times. When designing a point absorber-type wave energy generator, the choice of control system has an important impact on improving the power generation efficiency in actual sea areas (Li et al., 2020). Furthermore, a point absorber wave energy converter (PA-WEC) is a type of WEC that directly uses the changes in the magnetic field caused by the relative motion of the coil and the floating moving part with permanent magnets to generate electricity (Murai and Sakamoto, 2022). The power generation of a multi-PA-WEC array can be maximised by employing analytical background and numerical methods for deriving the optimal control force parameters (Murai et al., 2021). However, point absorption-type WECs have a narrow frequency response and perform unsatisfactorily in realistic ocean conditions unless their motion is actively controlled (Hals et al., 2011).

MPC is applied to wave energy generation systems to deal with problems such as strong system dynamics and complex constraints. However, many existing MPC strategies do not consider terminal stability constraints or disturbance feedback mechanisms. The control structure relies mostly on open-loop prediction, lacking the ability to handle disturbances and uncertainties in a closed loop. This makes it difficult to ensure recursive feasibility during actual operation, potentially leading to unsolvable optimisation problems at certain times. The general approach is to design a robust MPC (RMPC) that ensures recursive feasibility for all possible realisations of stochastic uncertainty, either by adopting a min-max strategy for the worst-case evaluation of the cost function (Kothare et al., 1996) (Evans et al., 2014) or by parameterizing a partially separable feedback control law through a tube-based approach (Yu et al., 2013) (Lasheen et al., 2017). There is a conflict between maximizing captured energy and ensuring the range of sea conditions for the safe operation of the system. The trade-off between them is difficult to achieve and reduces the operating range and energy conversion efficiency (Zhan et al., 2019a). AHMPC develops an efficient cascade estimation algorithm at the top level to adaptively identify and update the WEC model online according to the sea state changes. At the bottom level, a specially customised MPC controller is implemented based on the updated WEC model to energy capture (Zhan et al., 2018). The economic feedback MPC control law includes the state feedback gain offline design to maximise the working range and online calculation to maximise capture energy (Zhan et al., 2019a) and optimise the energy conversion efficiency of WECs.

The control of WECs is a noncausal control problem that requires a lot of online computing, and future waves determine the current control decisions (Wang et al., 2024). The above methods cannot effectively alleviate the problem of excessive computational workload during the online calculation of WECs, and it remains a challenge to meet the real-time requirements. They are restricted when computing resources are limited, the computational demand is too high, and they have limited adaptability to dynamically changing sea conditions. This paper proposes an explicit model predictive control (EMPC) solution for the control problem of WECs. Based on multi-parameter planning technology, EMPC calculates the optimal control behaviour offline, expresses it as an explicit function, and predicts the future state of the system. When online, it is simplified to a regional piecewise linear controller to avoid online solutions. Each region corresponds to a different equation, and a simple function evaluation is performed to reduce a lot of computational burden while achieving rapid prediction and efficient optimisation (Bank et al., 1982) (Alessio and Bemporad, 2009). The disturbance observer and autoregressive model perform wave prediction to maximise energy. In the power sector, EMPC is applied to the frequency control of a real isolated power system in Inner Mongolia, and its explicit control law restores the system frequency to the nominal value under large disturbances (Jiang et al., 2016). When EMPC is applied to a hybrid battery-supercapacitor power supply, the EMPC system requires less computation than the traditional MPC system for low-order systems. When implemented on a DSPACE DS1104 controller board, the EMPC system operates approximately 25 times faster than the traditional MPC system (Hredzak et al., 2015). When EMPC is applied to a vehicle semi-active suspension system, it copes with the strong coupling, actuator constraints, and fast dynamic characteristics of the system. Simulation results show that EMPC has a shorter computation time than traditional MPC while maintaining the same performance as MPC. EMPC significantly improves the control performance of the vehicle semi-active suspension system with low computational effort (Houzhong et al., 2020). This paper aims to apply EMPC to the problem of WEC control for the first time. Many active control strategies require knowledge of the wave excitation forces acting on the WECs, which are usually assumed to be accurately known and require forward predictions of several seconds. These conditions are unrealistic for operating WECs, resulting in actual performance degradation. Therefore, when using EMPC, the control strategy must be robust to modelling errors and other uncertainties (Hillis et al., 2020). The main novelties and contributions of this paper are as follows:

1. EMPC is proposed to control WECs under complex constraints, reducing the number of online calculations of MPC and solving problems of optimal trajectory tracking, rapid prediction, and efficient optimisation. This is the first application of EMPC in WEC control.

2. In the EMPC application process, to achieve visualisation and reduce the computational effort, this paper adopts the balanced truncation method to reduce the order of the tenth-order model and achieve model matching, and uses the second-order model to equivalently replace the tenth-order model in the low-frequency range.
3. This paper designs a wave observer and an autoregressive model for wave prediction to achieve energy maximisation since WEC control is a noncausal control problem.
4. This article uses realistic wave data gathered from the coast of Cornwall, UK (Zhang et al., 2019) (Li and Belmont, 2014), to verify the effectiveness of EMPC in WEC control.

The paper proceeds as follows: Section II is the mathematical modelling of the WEC dynamic system. Section III analyses the EMPC for energy capture maximisation. Section IV presents the simulation results and analysis. Section V provides an overall conclusion of this paper.

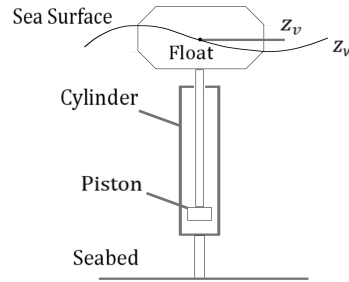


Figure 1: Schematic diagram of point absorber.

## 2. Mathematical Modelling of WEC Dynamic System

This section introduces the dynamic model of a single-point absorber. In Section 2.1, the hydrodynamic model is transformed into a state-space model to design the controller, which introduces modelling uncertainty. Section 2.2 presents the process of transforming the hydrodynamic model into a state-space model and model matching. Section 2.3 gives the optimal trajectory generation to the noncausal WEC control problem of an accurately modeled point absorber.

### 2.1. Dynamical Model of WECs

Figure 1 shows part of the hydraulic power take-off (PTO) design, where a hydraulic cylinder is mounted vertically below a float and fixed to the bottom of the seabed. More details of this design can be found in (Weiss et al., 2012).  $z_w$  is the sea wave elevation and  $z_v$  is the height of the midpoint of the float. The current research mainly considers the actual sea conditions in deep water and does not consider the shallow water conditions. In this environment, the PTO displacement of the WECs is usually regarded as the heave displacement  $z_v$ . The PTO torque is proportional to the force  $f_u$  acting on the piston in the cylinder. The output power  $P$  is defined as:

$$P := -f_u z_v \quad (1a)$$

The energy absorbed during the period  $[t_0, t_1]$  is expressed as:

$$E = \int_{t_0}^{t_1} P(t) dt \quad (1b)$$

The heave motion of the buoy is restricted to ensure safe operation. The constraint is expressed as:

$$|z_v| \leq \Phi_{\max} \quad (2a)$$

where  $\Phi_{\max}$  is the float heave motion limits. The WEC is subject to PTO force limitations:

$$|f_u| \leq u_{\max} \quad (2b)$$

The objective of the controller design is to maximise the energy (1b) subject to the state constraints (2a) and the input constraints (2b) (Zhan and Li, 2018). The dynamic equations (Yu and Falnes, 1995) for the float of the point absorber are given by Newton's second law:

$$m_s \ddot{z}_v = -f_s - f_r + f_e + f_u \quad (3)$$

where  $m_s$  is the float mass. The restoring force  $f_s$  is:

$$f_s = k_s z_v \quad (4)$$

where the hydrostatic stiffness is given by  $k_s = \rho g s$ ,  $\rho$  is the water density,  $g$  is the standard gravity, and  $s$  is the cross-sectional area of the float. The radiation force  $f_r$  is defined as:

$$f_r = m_\infty \ddot{z}_v + \int_{-\infty}^{\infty} h_r(\tau) \dot{z}_v(t - \tau) d\tau \quad (5)$$

where  $m_\infty$  is the added mass,  $h_r$  is the radiation force kernel, which can be computed via hydraulic software packages. The convolutional term in (5) can be approximated as  $f_r := \int_{-\infty}^{\infty} h_r(\tau) \dot{z}_v(t - \tau) d\tau$  by a causal finite-dimensional state-space model (Yu and Falnes, 1995).

$$\dot{x}_r = A_r x_r + B_r z_v \quad (6a)$$

$$y_r = f_r = C_r x_r \approx \int_{-\infty}^t h_r(\tau) \dot{z}_v(t - \tau) d\tau \quad (6b)$$

where  $x_r \in \mathbb{R}^{n_r}$  is the state, and  $(A_r, B_r, C_r, 0)$  are the state-space realisations. According to (Yu and Falnes, 1995), the wave excitation force  $f_e$  can be determined:

$$f_e = \int_{-\infty}^{\infty} h_e(\tau) z_w(t - \tau) d\tau \quad (7)$$

where  $h_e$  is the kernel of the excitation force, and the state-space approximation is given by:

$$\dot{x}_e = A_e x_e + B_e z_w \quad (8a)$$

$$y_e = f_e = C_e x_e \approx \int_{-\infty}^{\infty} h_e(\tau) z_w(t - \tau) d\tau \quad (8b)$$

where  $x_e \in \mathbb{R}^{n_e}$  is the state, and  $(A_e, B_e, C_e, 0)$  are the state-space realisations.

## 2.2. State-space Model

With the realisations of (6a), (6b), (8a) and (8b), the state–space model of (3) can be represented by:

$$\dot{x} = A_c x + B_{uc} u + B_{wc} w + \epsilon \quad (9a)$$

$$y = C_c x \quad (9b)$$

where  $w := z_w$  is the wave elevation whose prediction is incorporated into the controller design,  $y := z_v$ ,  $x := [z_v, \dot{z}_v, x_r, x_e]$ , and  $u := f_u$ .  $\epsilon$  represents the model uncertainty caused by wave force approximations in equations (6b) and (8b). And

$$A_c = \begin{bmatrix} 0 & 1 & 0 & 0 \\ -\frac{k_s}{m} & -\frac{D_f}{m} & \frac{C_r}{m} & -\frac{C_e}{m} \\ 0 & B_r & A_r & 0 \\ 0 & 0 & 0 & A_e \end{bmatrix} \quad B_{uc} = \begin{bmatrix} 0 \\ \frac{1000}{m} \\ 0 \\ 0 \end{bmatrix} \quad B_{wc} = \begin{bmatrix} 0 \\ 0 \\ 0 \\ B_e \end{bmatrix} \quad C_c = [0 \quad 1 \quad 0_{1 \times (n_e + n_r)}]$$

with  $m := m_s + m_\infty$ . The balanced truncation method is used to reduce the order of the tenth-order model and verify the model's matching. The parameters are gradually optimised to establish a second-order model to achieve an equivalent replacement for the tenth-order model in the low-frequency range:

$$A_c = \begin{bmatrix} 0 & 1 \\ -\frac{k_s}{m} & -\frac{D_f}{m} \end{bmatrix} \quad B_{uc} = \begin{bmatrix} 0 \\ \frac{1}{m} \end{bmatrix} \quad B_{wc} = \begin{bmatrix} 0 \\ \frac{D_e}{m} \end{bmatrix} \quad C_c = [0 \quad 1]$$

The continuous-time model (9a) and (9b) can be converted to a discrete-time model (10a) and (10b).

$$x_{k+1} = Ax_k + B_u u_k + B_w w_k + \epsilon_k \quad (10a)$$

$$y_k = Cx_k \quad (10b)$$

where the quadruple  $(A, B_u, B_w, C)$  is the discrete-time form of the quadruple  $(A_c, B_{uc}, B_{wc}, C_c)$ .

The balanced truncation method was first proposed by Moore (1981) and is an effective model simplification method for linear systems. In the balanced truncation process, high-dimensional stable structures may be both controllable and observable. In most cases, a transformation is established, as described in Moore (1981), which transforms the system into a unique form where the controllability and observability Gramians are equal. This produces a diagonal matrix  $\Sigma$  with the Hankel singular values on the diagonal arranged in descending order of dominance (Suman and Kumar, 2021). For nonlinear systems, balanced truncation based on algebraic Gramians can be achieved by solving Lyapunov-type equations (Gray and Verriest, 2006).

To reduce the computational demand of the tenth-order model and allow EMPC to operate on offshore devices with limited capability, the balanced truncation method is introduced to reduce the order of the tenth-order model. The order of the reduced-order model is second order. The main dynamic and energy capture characteristics of the tenth-order model are preserved, ensuring that the reduced-order model remains highly consistent with the tenth-order model in terms of position and energy capture. The performance of the reduced-order model closely matches that of the tenth-order model in terms of dynamic response, velocity, and PTO force.

A second-order model is established by optimizing parameters and compared with reduced-order and tenth-order models. The second-order model achieves performance nearly identical to the tenth-order model in terms of position and energy. In terms of velocity and PTO force, it shows a higher approximation than the reduced-order model, aligning more closely with the tenth-order model. The second-order model accurately captures the key dynamic behaviours of the system and achieves an equivalent replacement for the tenth-order model, which significantly reduces the computational demand. To verify the effectiveness of the reduced-order model, comparison results in both the frequency and time domains are shown in the simulation section, demonstrating model matching verification after reduction from the tenth-order model and the equivalent substitution achieved by the second-order model.

### 2.3. Optimal Trajectory Generation

This paper uses EMPC to track the optimal trajectory and maximise energy capture. The optimal trajectory of WECs is:

$$\min_u \frac{1}{N} \sum_{k=0}^{N-1} L_k(x_k, u_k) \quad (11a)$$

s.t.

$$x_{k+1} = Ax_k + B_u u_k + B_w w_k \quad (11b)$$

$$y_k = C_c x_k \quad (11c)$$

where  $N$  is the number of prediction steps and  $L_k$  is the stage cost:

$$L_k = \frac{1}{2} x_k^T Q' x_k + y_k u_k + \frac{1}{2} R' u_k^2 \quad (12)$$

where  $\frac{1}{2} x_k^T Q' x_k$  represents the weighted penalty term on the system state,  $Q'$  and  $R'$  are positive definite matrices,  $Q'$  influences the stability of the control system and serves as a tuning parameter for addressing state constraints (2a),  $-y_k u_k$  represents the power that the power take-off (PTO) mechanism can capture, minimizing  $y_k u_k$  is maximizing energy output,  $\frac{1}{2} R' u_k^2$  is introduced to penalise the input,  $R'$  affects the stability of the control system, and is a tuning parameter for handling the input constraint (2b) (Zhan and Li, 2018).

## 3. Explicit MPC for Energy Maximisation

This section describes the proposed EMPC. Section 3.1 introduces the overall strategy of the proposed controller. In Section 3.2, EMPC is used to achieve optimal trajectory tracking and maximise energy capture. Section 3.3 presents the design of the disturbance observer. Section 3.4 presents the wave prediction through the autoregressive model.



All parameters of the system (mass, stiffness, and damping) are measured and determined. The motion of the floating object is described by Newton's second law, and the position and velocity are defined as state variables to establish the dynamic model of the floating object, and its equation is given by:

$$m\ddot{z} = -k_s z - D_r \dot{z} + D_e \quad (17)$$

where  $m = m_s + m_\infty$  is the total mass of the floating object, including the mass of the floating body  $m_s$  and the added mass  $m_\infty$ ,  $z$  is the displacement of the floating object on the water surface,  $\dot{z}$  is the velocity of the floating object,  $\ddot{z}$  is the acceleration of the floating object,  $k_s$  is the stiffness parameter of the system,  $D_r$  is the damping coefficient, and  $D_e$  is the external excitation force on the system.

EMPC controls the position and velocity of the float so that it follows  $z_*$  and  $v_*$ .  $x_{\text{pred}}$  is  $[z_{\text{pred}}, v_{\text{pred}}]$ . The position and velocity are represented by  $z_{\text{pred}}$  and  $v_{\text{pred}}$ , respectively. The system considers the desired state, excitation force, white noise interference, and model uncertainty when performing control. The discrepancies between  $z_{\text{pred}}$  and  $z_*$ , as well as between  $v_{\text{pred}}$  and  $v_*$ , are considered as errors:

$$z_{\text{err}} = z_* - x_{\text{pred}}(1) \quad (18)$$

$$v_{\text{err}} = v_* - x_{\text{pred}}(2) \quad (19)$$

EMPC controls error, and the generated PTO force is denoted as  $u_{\text{err}}$ . The PTO force limit is given by:

$$u_{\text{err}} = \min(\max(u_{\text{err}}, -u_{\text{max}}), u_{\text{max}}). \quad (20)$$

For each time step  $k$ , the PTO force  $u_{\text{pred}}$  is given by:

$$u_{\text{pred}} = u_{\text{err}} + U_{\text{loc}}(k) \quad (21)$$

where  $U_{\text{loc}}$  is the PTO force of the optimal model and  $u_{\text{pred}}$  is the PTO force of the predicted model.

The powers of noncausal and causal control are defined as  $P_{\text{loc}} = -u_{\text{loc}} y_{\text{loc}} T_s$  and  $P_{\text{cau}} = -u_{\text{cau}} y_{\text{cau}} T_s$ , respectively, where  $u_{\text{loc}}$  and  $u_{\text{cau}}$  are the PTO force under noncausal and causal control, and  $y_{\text{loc}}$  and  $y_{\text{cau}}$  are the velocity under noncausal and causal control.  $T_s$  denotes the sampling interval. A negative value indicates energy consumption.

The cumulative energy of noncausal and causal control is given by  $E_{\text{loc}}(i) = E_{\text{loc}}(i-1) + P_{\text{loc}}(i)$  and  $E_{\text{cau}}(i) = E_{\text{cau}}(i-1) + P_{\text{cau}}(i)$ , where  $i$  denotes the time step. The instantaneous power at time  $i$ , denoted as  $P(i)$ , represents the rate of energy transfer caused by the PTO force  $u_{\text{loc}}$  and  $u_{\text{cau}}$ . The corresponding energy at time  $i$ , denoted as  $E(i)$ .

For both accurate and inaccurate models, the instantaneous powers at each time step  $i$  are given by  $P_{\text{loc}2}(i) = -u_{\text{loc}2}(i) y_{\text{loc}2}(i) T_s$  and  $P_{\text{loc}3}(i) = -u_{\text{loc}3}(i) y_{\text{loc}3}(i) T_s$ , where  $u_{\text{loc}2}$  and  $u_{\text{loc}3}$  represent the PTO forces and velocities in the accurate and inaccurate models, respectively.

The cumulative energies are obtained as  $E_{\text{loc}2} = \sum_{i=1}^{N_m} P_{\text{loc}2}(i)$  and  $E_{\text{loc}3} = \sum_{i=1}^{N_m} P_{\text{loc}3}(i)$ , respectively, where  $N_m$  denotes the total number of simulation steps. The time-varying cumulative energies  $E_{\text{loc}2}(i)$  and  $E_{\text{loc}3}(i)$  represent the energy accumulated at each time step  $i$  for the accurate and inaccurate models, respectively.

### 3.3. Disturbance Observer Design

A disturbance observer is designed to estimate the disturbance  $\hat{d}(t)$  in the system, where the controller uses the estimated disturbance to counteract its effects (Nian et al., 2020). The observer estimates the excitation force, and by accurately estimating the upper bound of the prediction error, the compensator effectively corrects the estimation error (Zhang et al., 2020). Linear feedback control requires a high gain to suppress the effects of model uncertainty and external disturbances (Zhang et al., 2017). An appropriate switching gain can prevent the jitter phenomenon associated with the traditional observer. The update of the disturbance estimation is given by:

$$\hat{d}_{k+1} = (1 - K_c) \hat{d}_k + K_e C_c x_{k,\text{pred}} - \beta \sum C_c x_{k,\text{pred}} \quad (22)$$

where  $\hat{d}_{k+1}$  is the estimated value of the disturbance at the next time step  $k+1$ ,  $\hat{d}_k$  is the estimated value of the disturbance at the current time step  $k$ ,  $K_c$  is the observer gain used to control the convergence velocity of the disturbance estimation term  $\hat{d}$ ,  $K_e$  is the gain used to adjust the error feedback,  $C_c$  is the output matrix, and  $\beta$  is the gain coefficient, which adjusts the error correction term. The wave is estimated by the disturbance observer, and the update of the disturbance observer is given by:

$$\hat{w} = C_c x_{\text{pred}} + \hat{d} \quad (23)$$

where  $\hat{w}$  is the estimated wave and  $\hat{d}$  is the disturbance estimation. The estimated value serves as an input for controller design. It is not practical to directly measure all states of the WECs. A state observer needs to be designed to solve this problem (Zhan et al., 2019b). The feedback noncausal MPC control algorithm is designed based on the assumption that all information about  $x_{\text{pred}}$  is available.

### 3.4. Wave Prediction by Autoregressive Model

Recursive least squares (RLS) is a commonly used parameter estimation algorithm Xiao et al. (2008), which is used to train an autoregressive model for wave data prediction to minimise the model error. The sampling time is  $T_s$ . The training segment duration of the model training is  $T_{\text{train}}$ . The prediction segment duration is  $T_{\text{predict}}$ . After each 5-second training cycle, a 1-second prediction is performed. The total prediction time is  $T_{\text{total}}$ . The number of prediction points in each prediction segment is  $N_{\text{pred}}$ . The training-prediction cycle time offset  $N_{\text{shift}}$  represents the time interval from training to prediction. The number of points in the prediction segment is  $N_{\text{shift}}$ . The initial regularisation coefficient is  $\alpha_{\text{base}}$ . To ensure a uniform scale of the training data, the data is normalised:

$$\tilde{w} = \frac{w - \mu}{\sigma} \quad (24)$$

where  $\tilde{w}$  is the standardised training value,  $\mu$  is the mean of  $w$ , and  $\sigma$  is the standard deviation of  $w$ . Before performing multi-step prediction, initialise an initial input vector  $\phi$  that contains past observations used for prediction. The input vector is represented as:

$$\phi = [\tilde{w}_{N_{\text{train}}} \quad \tilde{w}_{N_{\text{train}}-1} \quad \cdots \quad \tilde{w}_{N_{\text{train}}-p+1}]^T \quad (25)$$

where the first  $p$  data points are extracted from the training data and reversed to form the input vector  $\phi$  of the autoregressive model,  $p$  denotes the order of the autoregressive model, indicating that each prediction relies on  $p$  past data points. The predicted value is given by:

$$w_{\text{pred}} = \theta \phi \quad (26)$$

where  $\phi$  is the set of input vectors,  $w_{\text{pred}}$  is the predicted value, and the parameter vector  $\theta$  represents the weights of the model, its initial value set to the zero vector. Through the RLS algorithm,  $\theta$  is updated progressively to minimise the prediction error. The predicted error  $e_{\text{pred}}$  is given by:

$$e_{\text{pred}} = \tilde{w} - w_{\text{pred}} \quad (27)$$

where  $w_{\text{pred}}$  is the predicted value and  $e_{\text{pred}}$  is the predicted error, defined as the difference between the predicted value and the true value. By following these steps, obtain the multi-step prediction results over a specified time period:

$$\alpha_{\text{dynamic}} = \alpha_{\text{dynamic}}(1 + |e_{\text{pred}}|) \quad (28)$$

where the dynamic regularisation coefficient  $\alpha_{\text{dynamic}}$  is initially equal to  $\alpha_{\text{base}}$ ,  $\alpha_{\text{dynamic}}$  is adjusted at each step to control the strength of the updates and  $|e_{\text{pred}}|$  is the prediction error. When  $|e_{\text{pred}}|$  is large, the regularisation coefficient is amplified to reduce the magnitude of parameter updates. The Kalman gain  $K$  is given by:

$$K = \frac{P\phi'}{\lambda_{\text{rls}} + \phi P \phi' + \alpha_{\text{dynamic}} + l} \quad (29)$$

where  $P\phi'$  represents the incremental information from the past, and the denominator includes the forgetting factor  $\lambda_{\text{rls}}$  and the regularisation term to ensure stable updates.  $\lambda_{\text{rls}}$  attenuates the influence of old data,  $P$  is the covariance matrix used for updating the parameter calculations, and  $l$  is the regularisation parameter used to prevent overfitting. The parameter update equation for the parameter  $\theta$  is given by:

$$\theta_k = \theta_{k-1} + K e_{k,\text{pred}} \quad (30)$$

The update equation for the covariance matrix  $P$  is given by:

$$P_k = \frac{(1 - K\phi_{k-1})P_{k-1}}{\lambda_{\text{rls}}} \quad (31)$$

where  $P$  gradually converges as time progresses, reducing the model's sensitivity to historical data and enhancing the stability and accuracy of predictions.

$$E_{\text{cv}}^{(p)} = \frac{1}{N_{\text{train}} - p} \sum_{k=p+1}^{N_{\text{train}}} |e_{\text{pred}}| \quad (32)$$

where  $E_{cv}^{(p)}$  denotes the cross-validation error of the autoregressive model with the order  $p$ , used to measure the model fitting performance at different orders: a smaller value indicates better model fitting,  $N_{\text{train}}$  is the total number of samples in the training data,  $N_{\text{train}} - p$  is the number of observations used to compute the error,  $k$  is an index variable used to iterate over the samples in the training dataset with a range from  $p + 1$  to  $N_{\text{train}}$ , ensuring sufficient historical data is available for prediction, and  $|e_{\text{pred}}|$  represents the absolute error between the predicted and true value.

Traditional modelling sequential estimation methods include the Akaike Information Criterion (AIC) and Bayesian Information Criterion (BIC) (Atyabi et al., 2016). AIC avoids overfitting and penalises complex models by balancing goodness of fit and model complexity:

$$AIC_p = N_{\text{train}} \log \left( \frac{1}{N_{\text{train}}} \sum_{k=p+1}^{N_{\text{train}}} e_{\text{pred}}^2 \right) + 2p \quad (33)$$

$$BIC_p = N_{\text{train}} \log \left( \frac{1}{N_{\text{train}}} \sum_{k=p+1}^{N_{\text{train}}} e_{\text{pred}}^2 \right) + p \log(N_{\text{train}}) \quad (34)$$

where  $AIC_p$  and  $BIC_p$  denote the AIC value and the BIC values, respectively, for a model with order  $p$ , a smaller value indicates a better-fitting model,  $N_{\text{train}}$  is the number of training samples,  $\log$  is used to capture data growth rates and assess model complexity,  $\sum_{k=p+1}^{N_{\text{train}}} e_{\text{pred}}^2$  denotes the total squared prediction errors,  $2p$  is the penalty term for model complexity in AIC, and  $p \log(N_{\text{train}})$  is the penalty term in BIC, which increases with the sample size. It indicates that higher-order models receive stronger penalties under BIC, which thus tends to choose simple models to avoid overfitting. BIC is stricter than AIC in penalizing complex models.

To perform multi-step prediction, the first predicted value  $\hat{w}_{1,\text{pred}}$  is appended to the input vector  $\phi_{\text{pred}}$  and used as the most recent observation for subsequent multi-step predictions:

$$\phi_{\text{pred}} = [\hat{w}_{1,\text{pred}} \quad \tilde{w}_{N_{\text{train}}} \quad \tilde{w}_{N_{\text{train}}-1} \quad \cdots \quad \tilde{w}_{N_{\text{train}}-p+2}]^T \quad (35)$$

Using the parameter vector  $\theta$  and the input vector  $\phi_{\text{pred}}$ , multi-step prediction is performed. The model output  $\hat{w}_{\text{pred}}$  is calculated as follows:

$$\hat{w}_{\text{pred}} = \theta \phi_{\text{pred}} \quad (36)$$

where  $\hat{w}_{\text{pred}}$  represents the predicted normalised value. To predict values for multiple time steps, the prediction output is repeated, and the input vector is updated at each prediction step  $k$ :

1. Generate the new prediction (36).
2. Update  $\phi_{\text{pred}}$ :

$$\phi_{\text{pred}} = [\hat{w}_{1,\text{pred}} \quad \phi_{1:\text{end}-1,\text{pred}}]^T \quad (37)$$

where the input vector  $\phi_{\text{pred}}$  contains the most recent predicted value along with the previous actual observations. After performing multi-step predictions, this paper denormalises the predicted results to convert the normalised predictions back to the original scale:

$$\bar{w} = \hat{w}_{\text{pred}} \sigma + \mu \quad (38)$$

where  $\bar{w}$  is the prediction result after denormalisation. If it is the first prediction, the predicted segment is directly appended to the total prediction results. Otherwise, to ensure continuity, the first value of the new segment is set to the last predicted value of the previous segment, and the segments are concatenated:

$$w_{p,\text{all}} = [w_{p,\text{all}}, \bar{w}] \quad (39)$$

where  $w_{p,\text{all}}$  represents the cumulative predicted value. After each prediction, the timestamp is updated:

$$t_{p,\text{all}} = [t_{p,\text{all}}, t_{\text{pi}}] \quad (40)$$

where  $t_{p,\text{all}}$  is a cumulative predicted time, and  $t_{\text{pi}}$  is the time series of the current predicted segment.

---

**Algorithm 1** Implementation of the WEC control
 

---

- 1: Obtain the system state  $x$  and the wave  $w$ .
  - 2: The EMPC generates the error PTO force  $u_{\text{err}}$ . The optimal model provides the PTO force  $U_{\text{loc}}$ . The predicted PTO force  $u_{\text{pred}}$  is obtained based on the equation (21).
  - 3: The predicted system state  $x_{\text{pred}}$  is the sum of the state error  $x_{\text{err}}$  and the system state  $x$ . The energy of the accurate and inaccurate models is captured in  $E_{\text{loc}2}$  and  $E_{\text{loc}3}$ , respectively.
  - 4: The disturbance observer generates an estimated wave  $\hat{w}$  in (23). The autoregressive model generates the predicted wave  $\hat{w}_{\text{pred}}$  in equation (36).
  - 5: Repeat steps 1 to 4.
- 

#### 4. Simulation Results and Analysis

This section shows the simulation results generated using MATLAB R2023b. The computer model is the Lenovo ThinkPad X13 Gen 2. This paper uses real wave data collected from the coast of Cornwall, UK. The wave heights from 0 to 200 seconds are shown in Figure 3, and the physical parameters are listed in Table 1. The significant wave height of the wave is 2.003m. The wave period range is 1.40 seconds to 10.80 seconds. The average wave period is 5.791 seconds. The model's natural period of the system is 24.1213 seconds. The model's natural period of the system is larger than the wave period range. Because the wave frequency is lower than the natural frequency of the system, the system does not resonate. This avoids loss of stability and generation of a large response. The operations of standard MPC and EMPC are implemented using MATLAB R2023b. The results show that the running time of EMPC is 61.16 seconds, while the running time of standard MPC is 926.64 seconds. Compared with MPC, EMPC has higher computational efficiency while maintaining similar control performance.

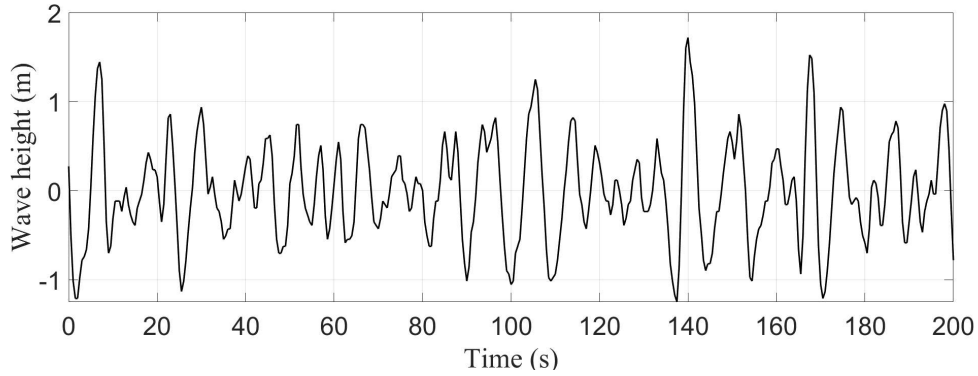


Figure 3: Wave height data gathered from the coast of Cornwall, UK (Zhang et al., 2019) (Li and Belmont, 2014).

The state space matrix of the impulse function for calculating the radiation force is:

$$A_r = \begin{bmatrix} 0 & 0 & -17.9 \\ 1 & 0 & -17.7 \\ 0 & 1 & -4.41 \end{bmatrix} \quad B_r = \begin{bmatrix} 36.5 \\ 394 \\ 75.1 \end{bmatrix} \quad C_r = [0 \quad 0 \quad 1]$$

The state space matrix of the impulse function for calculating the wave excitation force is:

$$A_e = \begin{bmatrix} 0 & 0 & 0 & 0 & -400 \\ 1 & 0 & 0 & 0 & -459 \\ 0 & 1 & 0 & 0 & -226 \\ 0 & 0 & 1 & 0 & -64 \\ 0 & 0 & 0 & 1 & -9.96 \end{bmatrix} \quad B_e = \begin{bmatrix} 1549886 \\ -116380 \\ 24748 \\ -644 \\ 19.3 \end{bmatrix} \quad C_e = [0 \quad 0 \quad 0 \quad 0 \quad 1]$$

The accurate and inaccurate  $Q$  and  $R$  are:

$$Q_{\text{acc}} = \begin{bmatrix} 10^1 & 0 \\ 0 & 10^1 \end{bmatrix} \quad Q_{\text{inacc}} = \begin{bmatrix} 10^1 & 0 \\ 0 & 10^1 \end{bmatrix} \quad R_{\text{acc}} = 10^{-3} \quad R_{\text{inacc}} = 10^{-3}$$

Table 1: Physical parameters of wave energy devices.

Description	Notation	Value
Physical parameters	$T_s$	0.1 s
Gravity acceleration	$g$	9.8 m/s <sup>2</sup>
Radius	$r$	0.35 m
Average density of seawater	$\rho$	1025 kg/m <sup>3</sup>
Total mass	$m$	325.5 kg
Stiffness	$k_s$	3866 N/m
Damping coefficient	$D$	$2 \times 10^5$ N · s/m
Damping (viscous)	$D_v$	0
Damping (friction)	$D_f$	0
Device width	$D_w$	0.7m
Prediction time	$P_{\text{time}}$	50 s
Prediction Steps	$P_{\text{step}}$	500 steps

White noise interference comes from environmental fluctuations and measurement errors. The system resists this interference through robust control, which helps maintain stability in complex environments. Parameter variations lead to deviations between expected and actual system behaviour. The control strategy takes these uncertainties into account and adjusts the inputs in real time. White noise is defined as:  $\epsilon = c\sigma'$ , where  $\epsilon$  represents white noise,  $c$  is the colored noise, and  $\sigma'$  is the time-varying standard deviation.

Wave energy systems usually work in the low-frequency range, where most of the energy is concentrated. Therefore, the dynamic behaviour of the system is primarily dominated by low-frequency characteristics. Based on this, the balanced truncation method is introduced to reduce the tenth-order model into a reduced-order model of second order. Figure 4 demonstrates the Bode diagrams of both the tenth-order and reduced-order models. The amplitude responses of the two models show a close match in the frequency range of 0.1 to 1 rad/s, indicating that the reduced-order model effectively preserves the gain characteristics of the original system. Although there are some deviations in the phase response, especially at lower frequencies, the overall phase trend remains consistent, which demonstrates that the reduced-order model can accurately capture the essential dynamic behaviour of the original system and is suitable for subsequent analysis and control design.

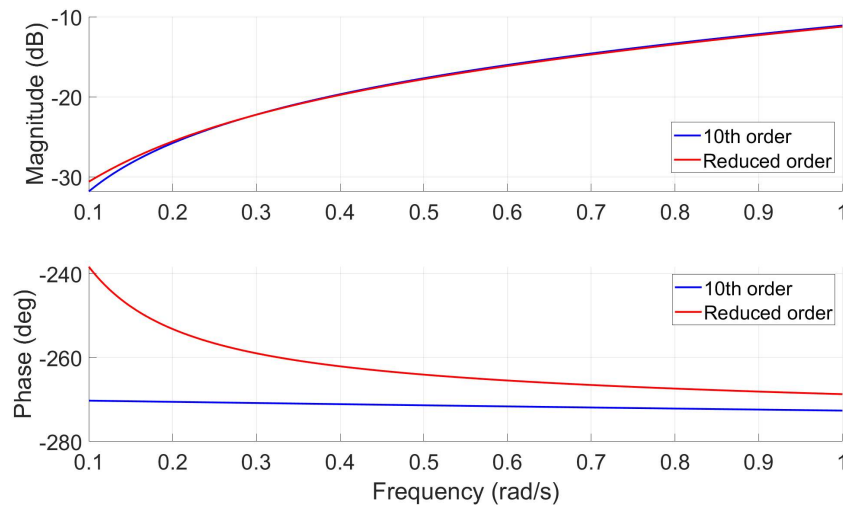


Figure 4: Bode diagram for model fidelity check.

On this basis, the second-order model is constructed by gradually adjusting the parameters. By comparing key output indicators such as displacement, velocity, control input, and energy, it is verified that the second-order model, reduced-order model, and tenth-order model have high consistency in time domain response, as shown in Figure 5.

The second-order model is highly consistent with the reduced-order and tenth-order models in key aspects such as energy transfer and system response, successfully capturing the primary dynamic behaviour of the system within the low-frequency range. Without losing the important characteristics of the system, the computational demand of the model is simplified, and the corresponding parameters are determined. Based on the verification and comparison of low-frequency matching and time-domain response, it is fully demonstrated that the second-order model can effectively achieve equivalent substitution for both the reduced-order model and the tenth-order model in terms of dynamic behaviour within the low-frequency range.

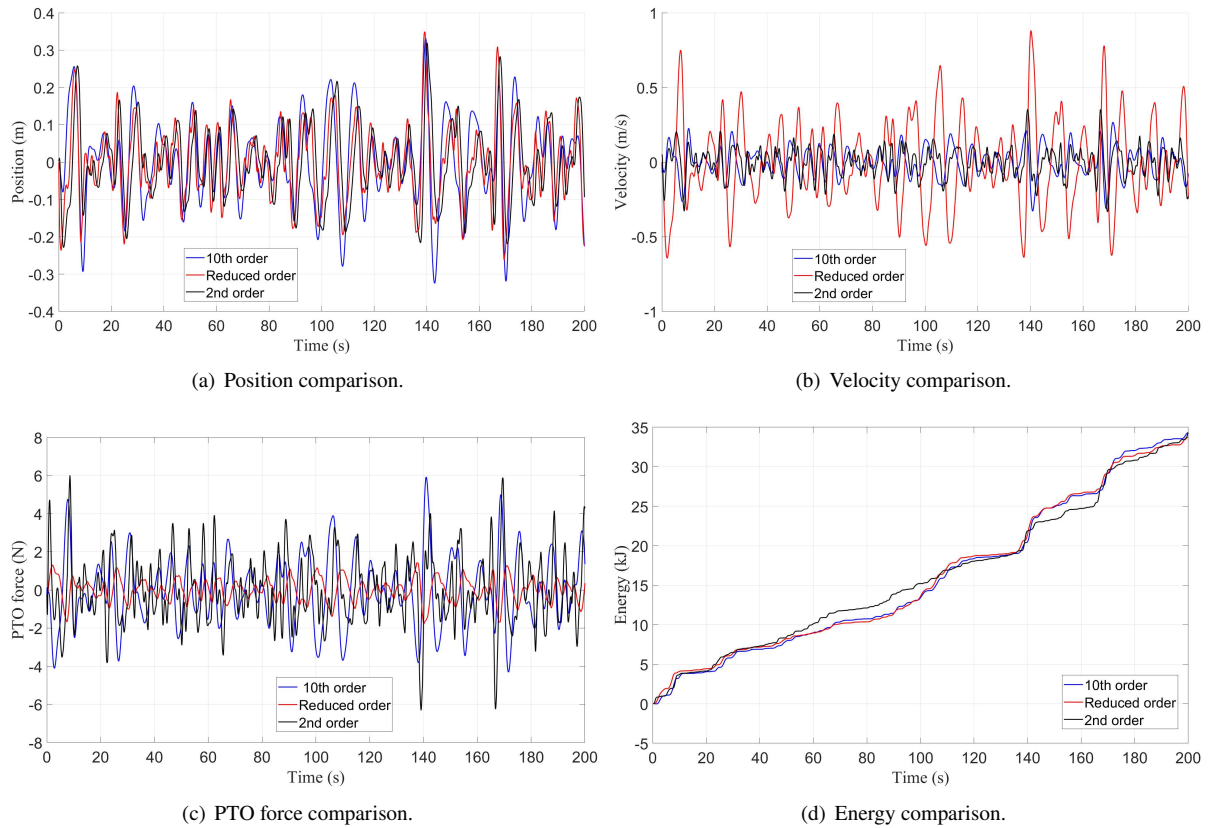


Figure 5: (a) Position comparison. (b) Velocity comparison. (c) PTO force comparison. (d) Energy comparison. Blue solid line: tenth-order model. Black solid line: second-order model. Red solid line: reduced-order model.

Energy and PTO force are shown in Figure 6. Energy output increases with the wave's energy content. The noncausal system accumulates more energy than the causal system does. The PTO force is constrained to an upper limit of 6 Newtons.

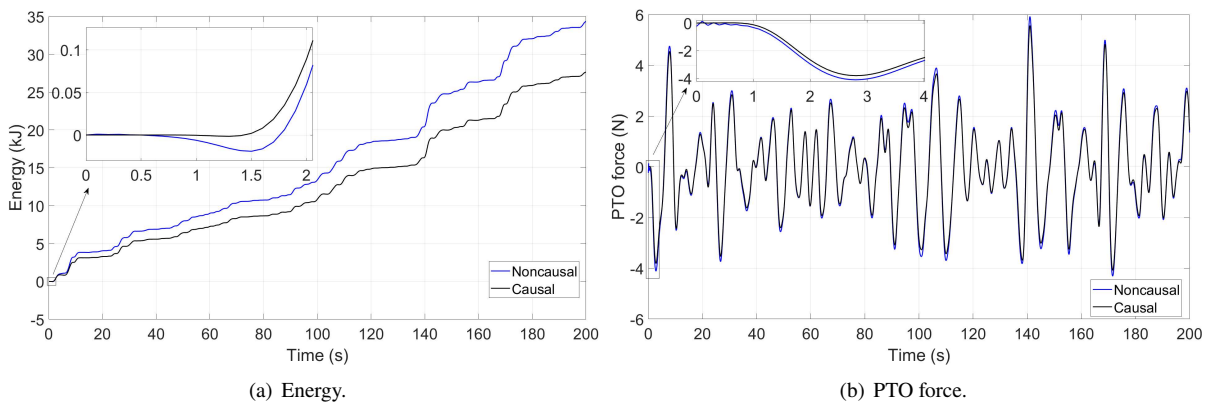


Figure 6: (a) Energy. (b) PTO force. Blue solid line: noncausal model. Black solid line: causal model.

Figure 7 demonstrates the energy and power comparisons. The accurate model captures more energy than the inaccurate model. The accurate model achieves the best energy capture effect, and the model accuracy has a clear positive impact on the control effect. Although the energy capture performance of the inaccurate model is reduced due to modelling errors and differs from the accurate model, the overall energy capture effect is still within an acceptable range. The power ranges from  $-0.05$  to  $0.25$ , following a similar trend, with the accurate model having higher power than the inaccurate model. Figure 8 demonstrates the position error and velocity error of the model. The position error ranges between  $-0.04$  and  $0.04$ , while the velocity error ranges between  $-0.06$  and  $0.08$ . The errors fluctuate within the acceptable range. Figure 9 demonstrates that the accurate and inaccurate models have similar PTO forces and consistent model training processes. The accurate model is more suitable for applications with high requirements for energy capture efficiency and control accuracy. Although the inaccurate model has a certain deviation from the accurate model, the control performance still meets the actual needs. The EMPC strategy demonstrates excellent fault tolerance and robustness in the application. Furthermore, it effectively addresses modelling uncertainty, which contributes to improving the applicability and operational stability of the system.

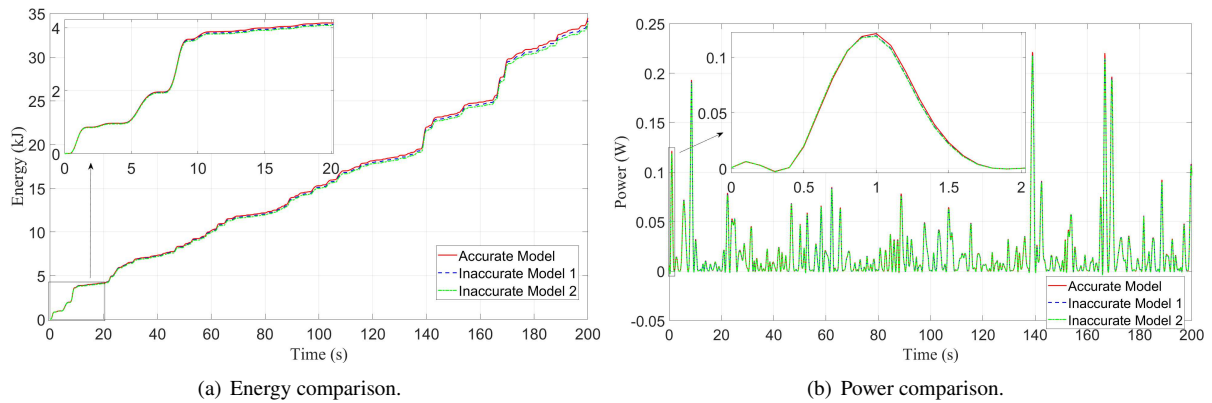


Figure 7: (a) Energy comparison. (b) Power comparison. Red solid line: accurate model. Blue dashed line: inaccurate model 1. Green dashed line: inaccurate model 2.

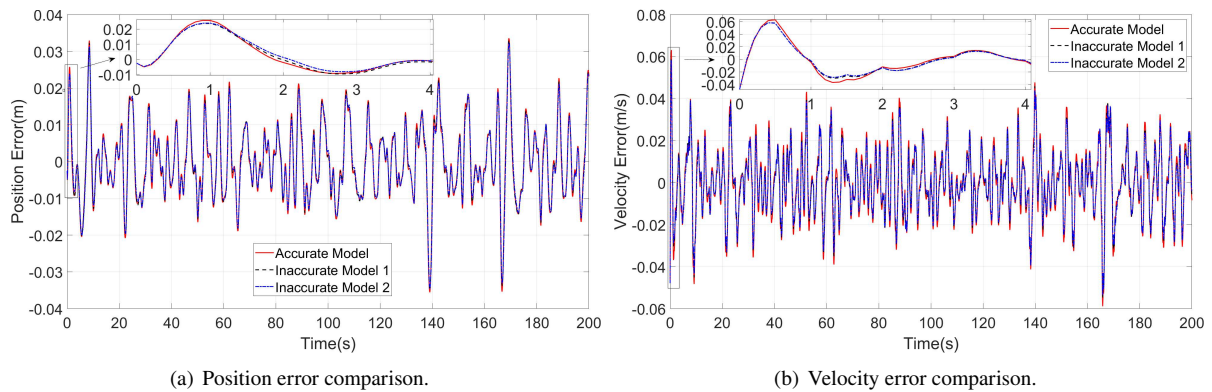


Figure 8: (a) Position error comparison. (b) Velocity error comparison. Red solid line: accurate model. Black dashed line: inaccurate model 1. Blue dashed line: inaccurate model 2.

Figure 10 demonstrates the partitioning of the system. The regional piecewise linear controller adopts corresponding control strategies in different regions based on the partitioning. Each region uses a specific calculation equation, which significantly reduces the computational burden. The partitioning range of the accurate model and the inaccurate model is the same, but the number of regions is different. The accurate model includes 111 regions, while the inaccurate model includes 109 regions. Both use similar control strategies in most regions, and there are differences only in a few regions.

The Monte Carlo method is used to set different initial predicted positions and initial predicted velocities, and multiple sets of predicted positions and predicted velocities are generated for comparison. From Figure 11 and Figure 12, based on the comparison of the position tracking and velocity tracking results of the accurate and

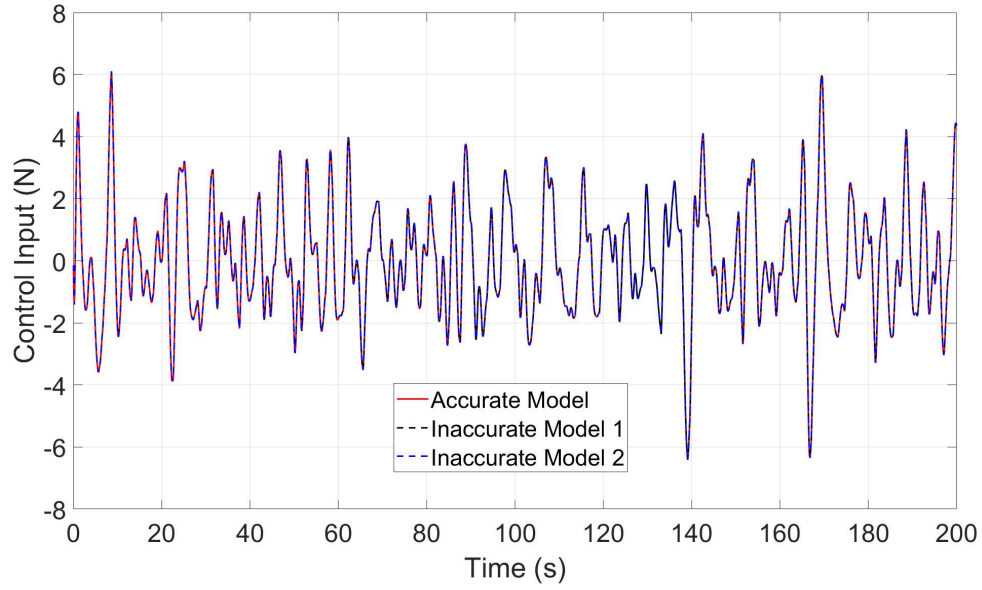


Figure 9: PTO force comparison. Red solid line: accurate model. Black dashed line: inaccurate model 1. Blue dashed line: inaccurate model 2.

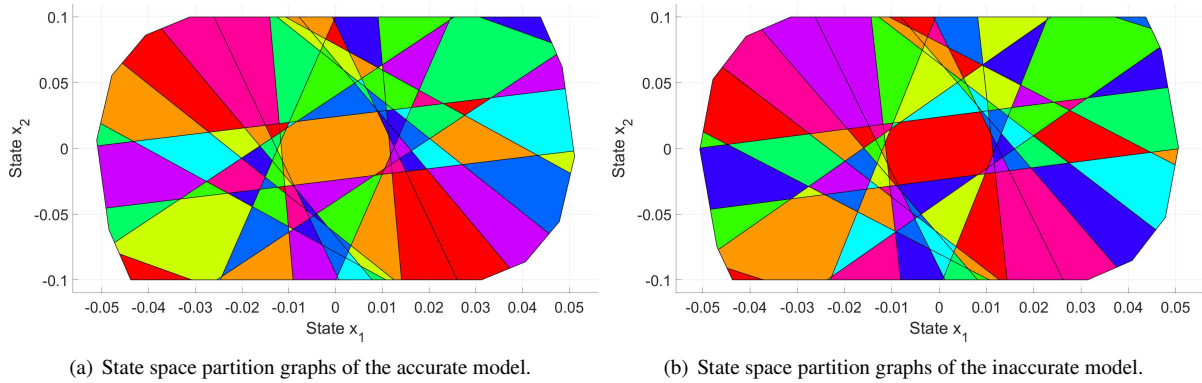


Figure 10: (a) State space partition graphs of the accurate model. (b) State space partition graphs of the inaccurate model.

inaccurate models, it can be observed that no matter what initial point the predicted position and velocity start from, the predicted results are eventually close to the position and velocity of the float. This shows that the system has an impressive ability to track the position and velocity of the float. The WEC parameters of the accurate and inaccurate models are shown in Table 2.

Table 2: WEC parameters of accurate model and inaccurate model.

Description	Notation	Value
Stiffness	$K_s^{\text{acc}}$	3866 N/m
Float mass	$m_s^{\text{acc}}$	320 kg
Added mass	$m_\infty^{\text{acc}}$	5.5 kg
Total mass	$m_{\text{acc}}$	325.5 kg
Radiation coefficient	$D_r^{\text{acc}}$	1000 kg/s
Excitation coefficient	$D_e^{\text{acc}}$	676 kg/s <sup>2</sup>

Description	Notation	Value 1	Value 2
Stiffness	$K_s^{\text{inacc}}$	3750 N/m	3800 N/m
Float mass	$m_s^{\text{inacc}}$	295 kg	300 kg
Added mass	$m_\infty^{\text{inacc}}$	2 kg	3 kg
Total mass	$m_{\text{inacc}}$	297 kg	303 kg
Radiation coefficient	$D_r^{\text{inacc}}$	970 kg/s	990 kg/s
Excitation coefficient	$D_e^{\text{inacc}}$	656 kg/s <sup>2</sup>	666 kg/s <sup>2</sup>

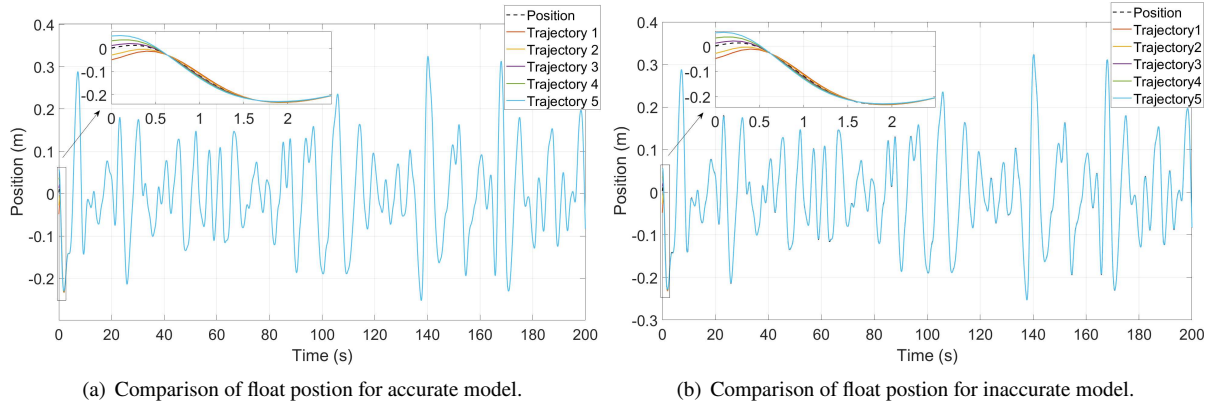


Figure 11: (a) Comparison of float position for an accurate model. (b) Comparison of float position for an inaccurate model. The float position is tracked from five different starting points.

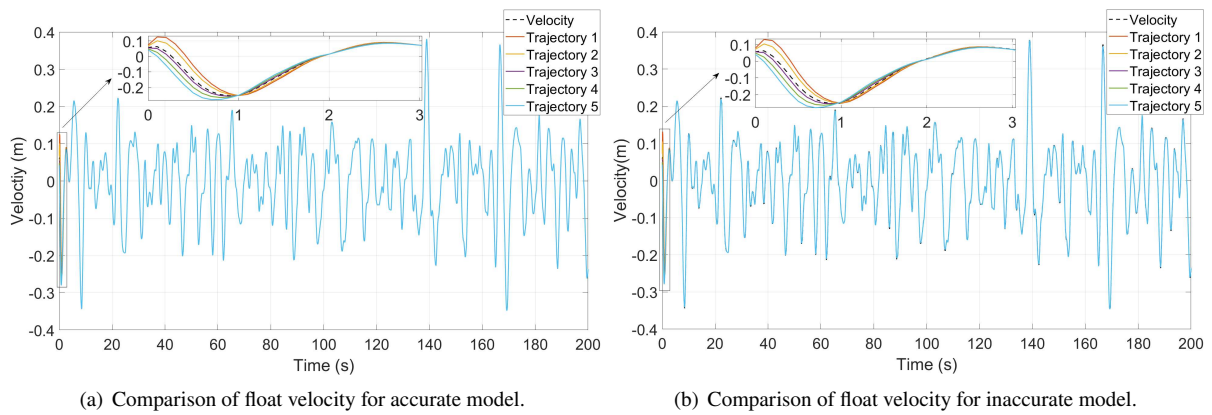


Figure 12: (a) Comparison of float velocity for an accurate model. (b) Comparison of float velocity for an inaccurate model. The float velocity is tracked from five different starting points.

In the three cases of  $Q$  and  $R$  in Table 3, the inaccurate model produces an energy of 34.3345 KJ. The model uses multi-parameter piecewise linear control segmentation, with case I involving 109 regions, and cases II and III both involving 163 regions. The results are shown in the Figure 13. Adjust the values of  $Q$  and  $R$  and perform multiple simulations. It is found that the final value of energy capture is affected by the values of  $Q$  and  $R$ . The final energy capture of Case I is 34.1534 KJ. The final energy capture of Case II is 34.2724 KJ. The final energy capture of Case III is 34.2690 KJ. Comparing Case I (green dashed line) and Case II (red dashed line), the larger the  $Q$  matrix value, the greater the energy capture. Comparing Case I (green dashed line) and Case III (blue dashed line), the larger the  $R$  value, the lower the energy capture. As the  $Q$  increases and  $R$  decreases, the number of regional divisions in the system partition diagram increases. The control strategy is more detailed, and the system's anti-interference ability is enhanced.

Table 3:  $Q$  and  $R$  three cases.

$Q$ and $R$	Case I	Case II	Case III
$Q_{\text{inacc}}$	$\begin{bmatrix} 10^1 & 0 \\ 0 & 10^1 \end{bmatrix}$	$\begin{bmatrix} 10^3 & 0 \\ 0 & 10^3 \end{bmatrix}$	$\begin{bmatrix} 10^1 & 0 \\ 0 & 10^1 \end{bmatrix}$
$R_{\text{inacc}}$	$10^{-3}$	$10^{-3}$	$10^{-5}$

Figure 14 demonstrates the comparison between the estimated wave and the wave height. It can be found that the estimated wave is similar to the wave height in amplitude and trend, with more fluctuations. Although there is a certain error, the estimation effect is well achieved. From Figure 15, the difference between the estimated wave and the predicted wave is compared. It can be seen that although there are certain errors, the overall trend is similar and

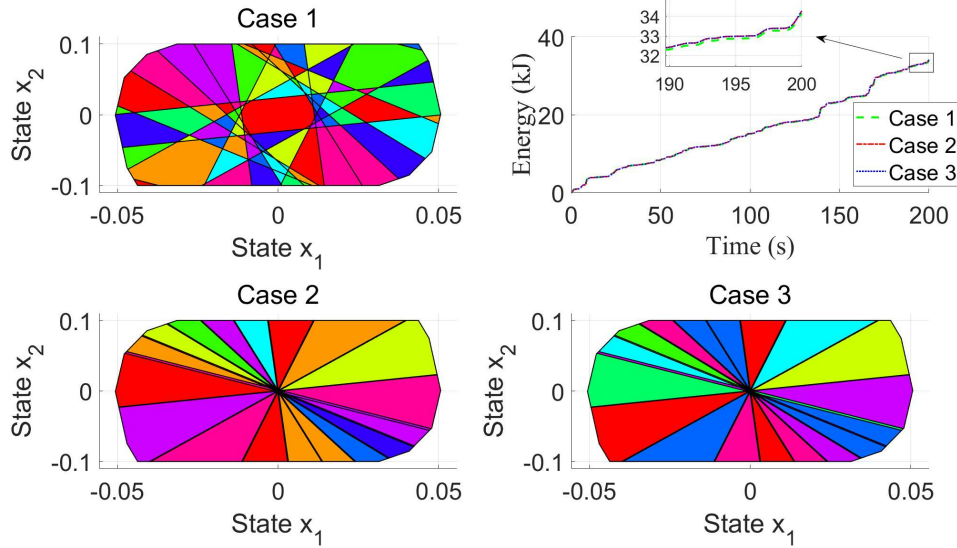


Figure 13: Comparison of energy and state space partitioning for three cases of  $Q$  and  $R$ . Green dashed line: first case. Red dashed line: second case. Blue dashed line: third case.

the error range is small, indicating that the prediction effect is impressive. The physical parameters of constraints, disturbance observer, and autoregressive model are shown in Table 4.

This study uses different wave data for testing. These waves are simulated using EMPC, and the corresponding energy output is generated. As shown in Figure 16, EMPC demonstrates impressive control and energy capture abilities under different wave conditions. This verifies its robustness and potential for practical application.

To compare the control performance under various sea conditions, wave profiles defined by significant wave height  $H_s$  and wave peak period  $T_p$  are simulated. The capture width ratio (CWR) is calculated to evaluate the energy conversion capability of the system in a real environment. The CWR is calculated as:  $CWR = \frac{P_{av}}{D_w \cdot P_w} \cdot P_{av}$  is the average mechanical power,  $D_w$  is the device width, and  $P_w$  is the wave power per meter of crest width. For the point absorber with parameters shown in Table 1, the device width is  $DW = 0.7m$ .

Figure 17 demonstrates the CWR of the point absorber obtained from a large-scale simulation under the JONSWAP (Joint North Sea Wave Project) wave model with a spectral peakedness factor of unity to generate irregular wavespectra (Zhang and Li, 2019). The significant wave heights are  $H_s = 1m$  and  $H_s = 1.5m$ , respectively. The wave crest period ranges from 1s to 12s with an interval of 1s. Model uncertainties and prediction errors are considered. The results show that the CWR shows a trend of increasing and then decreasing with the increase of the wave peak period. When the wave peak period is 4 seconds, the CWR reaches its maximum value. Then, as the wave peak period continues to increase, the CWR begins to decrease. Under different effective wave heights, the CWR maintains the same increasing and decreasing trend. The system's response under different wave heights generally exhibits a linear relationship, and the CWR values remain approximately consistent across varying wave height conditions. The proposed EMPC is able to cope with both prediction errors and model uncertainties in different ocean environments.

EMPC utilises multi-parametric quadratic programming to transform the online optimisation problem of traditional MPC into an equivalent, pre-computed piecewise explicit control law. At runtime, the appropriate control action is applied by identifying the region corresponding to the current system state, thereby eliminating the need to solve a quadratic programming problem at each time step. This significantly enhances real-time performance and computational efficiency.

Compared to traditional MPC, which depends on online optimisation, EMPC offers distinct advantages when applied to WEC systems:

1. Severe wave environment with high real-time control requirements:

The WEC system operates in a dynamic and uncertain marine environment. Rapid changes in waves cause drastic fluctuations in the system state, placing extremely high demands on the controller's real-time response capability. EMPC avoids the high computational burden of solving complex optimisation problems in real time by pre-calculating the control law offline. This method meets the stringent real-time control requirements of WEC systems and improves the dynamic performance and operational safety of the system.

2. Embedded platform with limited computing resources:

The WEC system mostly uses embedded microprocessors with limited computing resources. Traditional MPC relies on real-time quadratic programming solutions, which makes it difficult to meet the needs of high-frequency control under limited computing resources and energy consumption constraints. EMPC makes the control law explicit and realises fast calculation based on table lookup, significantly reduces the computational burden, and ensures the real-time operation of the controller on the embedded platform. EMPC expands the application of MPC in actual marine energy equipment.

### 3. Marine environment with predictable external disturbances:

When disturbances such as wave forces are effectively predicted through modelling and observation, EMPC fully considers the impact of disturbances when calculating the control law offline. This improves the robustness and stability of the control strategy in dynamic environments and further improves the energy capture efficiency and safety of equipment operation.

Although in recent years, a variety of research methods have been devoted to improving the performance of traditional MPC online solvers and have performed well in specific scenarios, such as the active-set method (Ricker, 1985) (Bemporad, 2015), the interior-point method (Wang and Boyd, 2009), the fast gradient-projection method (Patrinos and Bemporad, 2013), and the alternating direction method of multipliers (Banjac et al., 2017). However, for systems like WEC that have limited computational resources and are highly sensitive to control delays, EMPC has a clear advantage due to its explicit control law representation (Bemporad, 2021).

In summary, EMPC achieves an excellent balance between control performance and computational complexity. It is especially suitable for control environments with limited computing resources and strict requirements on the response time from state measurement to control execution, such as WEC systems. EMPC significantly reduces the online computational burden by pre-solving the control law offline, thereby improving the real-time security and stability of the system and providing solid technical support for the safe and efficient operation of the WEC system.

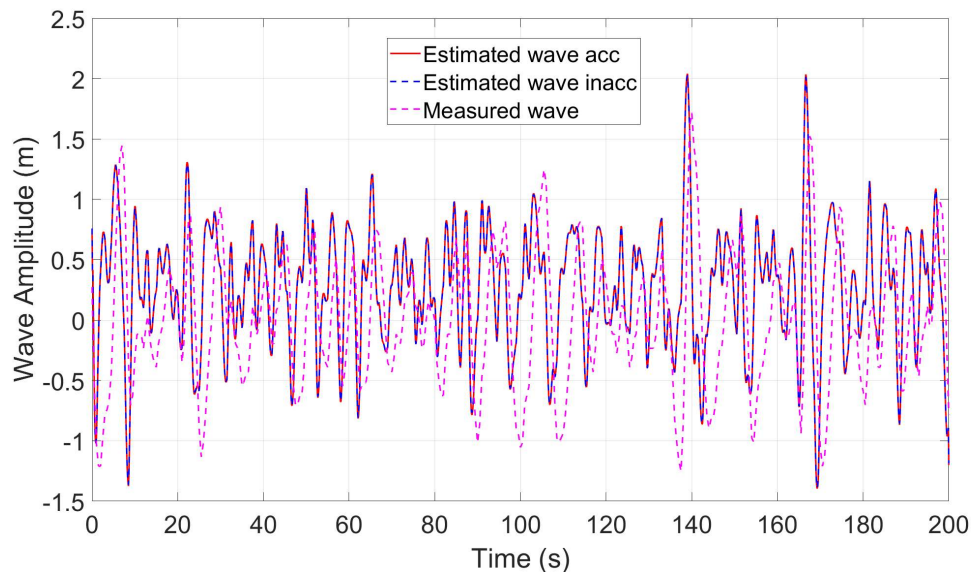


Figure 14: Wave height and estimated wave. Pink dashed line: wave height. Red solid line: estimated wave of the accurate model. Blue dashed line: estimated wave of the inaccurate model.

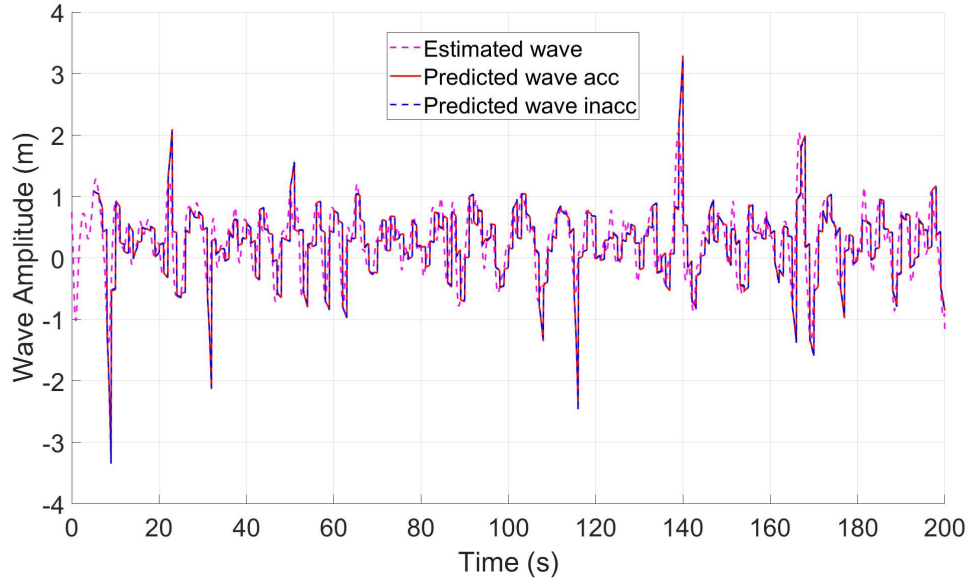


Figure 15: Estimated and predicted wave comparison. Pink dashed line: estimated wave. Red solid line: predicted wave of the accurate model. Blue dashed line: predicted wave of the inaccurate model.

Table 4: Physical parameters of constraints, disturbance observer, and autoregressive model.

Description	Notation	Value
Input force limit	$u_{\max}$	0.1 kN
Float heave coefficient	$z_{\max}$	0.1 m
Heave velocity limit	$v_{\max}$	0.1 m/s
Observer gain	$K_c$	1.5
Error feedback gain	$K_e$	6
Error correction gain	$\beta$	0.5
Forgetting factor	$\lambda_{\text{rls}}$	0.99
Initial regularisation coefficient	$\alpha_{\text{base}}$	$10^{-8}$
Regularisation parameter	$\ell$	$10^{-8}$
Sampling time	$T_s$	0.1 s
Training duration	$T_{\text{train}}$	5 s
Prediction duration	$T_{\text{predict}}$	1 s
Total prediction time	$T_{\text{total}}$	200 s
Prediction points	$N_{\text{pred}}$	11
Cycle time offset	$N_{\text{shift}}$	10
Covariance matrix	$P$	$10^7 \times I_p$
Identity matrix	$I_p$	$\begin{bmatrix} 1 & 0 & \cdots & 0 \\ 0 & 1 & \cdots & 0 \\ \vdots & \vdots & \ddots & \vdots \\ 0 & 0 & \cdots & 1 \end{bmatrix}_{p \times p}$

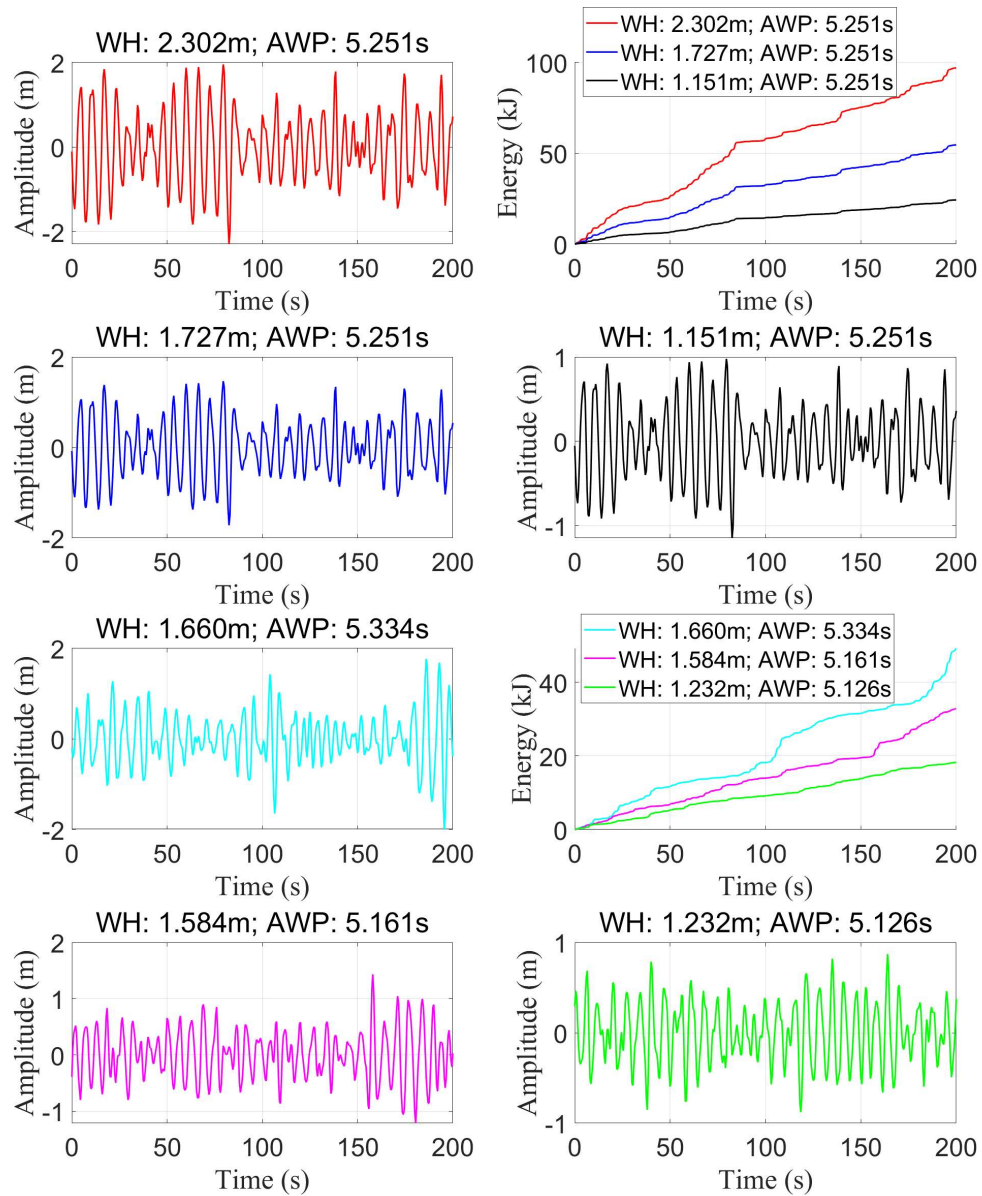
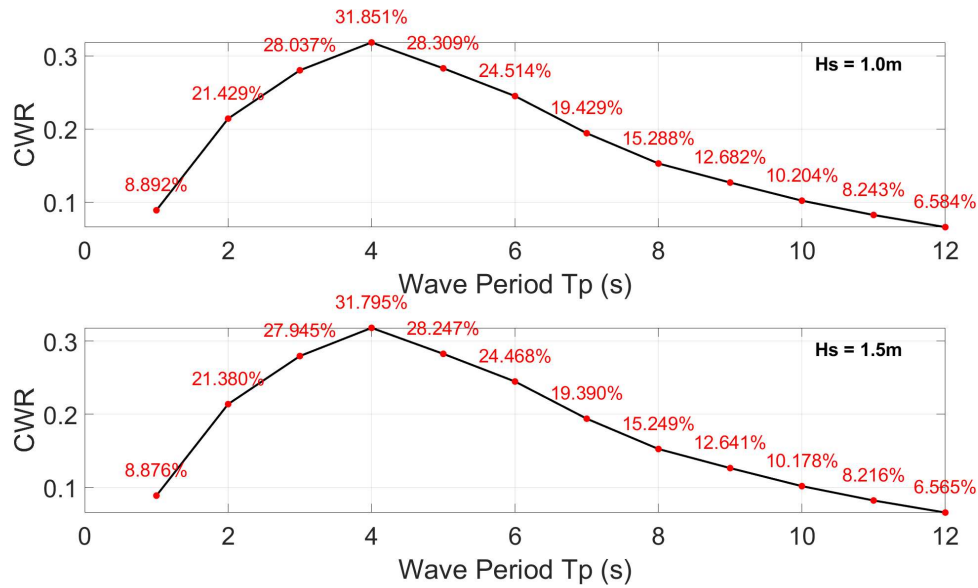


Figure 16: Energy comparison of different wave heights and average wave periods. WH is the wave height. AWP is the average wave period.


 Figure 17: Capture width ratio ( $H_s = 1m$  and  $H_s = 1.5m$ ).

## 5. Conclusions

For the control problem of wave energy converters (WECs), this paper has introduced explicit model predictive control (EMPC) for the first time, taking into account the computational limitations typical of embedded systems. A tenth-order system model was reduced using the balanced truncation method, and a second-order model was adopted as an equivalent substitute in the low-frequency range. A control performance comparison was conducted between accurate and inaccurate models of WECs, and the modelling error was subsequently established and controlled. Wave prediction was implemented using a disturbance observer in conjunction with an autoregressive model.

The results clearly demonstrated that the accuracy of the system model directly influences key performance indicators such as energy output, power, position, and velocity. A disturbance observer based on wave height was used for real-time state estimation and monitoring, while system parameters were identified using the RLS algorithm within the autoregressive model framework. Based on the estimated wave conditions, 1-second predictions were made following a 5-second learning period, with the wave data predicted in segments to reduce the computational burden.

The simulation results demonstrated that the EMPC method achieved excellent tracking performance in wave energy conversion, enabling fast operation and efficient optimisation of the system. This led to improved system performance and tracking accuracy, thereby enhancing the effective capture and utilisation of wave energy. These findings verify the importance of accurate modelling in WEC control and demonstrate that EMPC can maintain robust performance even in the presence of reasonable modelling errors.

In conclusion, this study has made significant advancements in the control of WEC through the application of EMPC. Compared to traditional control methods, EMPC effectively reduces the computational burden while maintaining a balance between rapid prediction and efficient optimisation under resource constraints and multiple system limitations. This approach ensures both high performance and real-time responsiveness.

EMPC is expected to enhance the efficiency of WECs, support the sustainable development and utilisation of wave energy, and maximise energy capture. By incorporating disturbance observers and autoregressive models, the system's ability to perceive and predict dynamic environmental changes was strengthened, enabling more accurate control.

Overall, this study focuses on achieving real-time EMPC implementation on platforms with limited computational resources and contributes to the broader adoption of intelligent control strategies in harsh marine environments.

While EMPC demonstrated strong control performance, it also has certain limitations. Its application has primarily been confined to linear systems, with control laws typically designed based on linear system models. This study extended the applicability of EMPC in practise by effectively controlling wave energy under varying wave heights, thereby achieving reliable energy capture and demonstrating its potential in practical scenarios.

Future work will focus on expanding EMPC to nonlinear systems and developing customised control strategies that reflect the dynamic characteristics of the system. The goal is to enhance the adaptability and reliability

of EMPC in complex engineering environments, while also improving computational efficiency and further reducing the computational burden. These advancements will support more robust system operation and improved adaptability under diverse operating conditions.

In addition, future research will explore the integration of EMPC with various renewable energy sources, such as wave energy, and undertake long-term reliability testing to validate the stability and effectiveness of EMPC-based systems in real-world environments.

## Acknowledgment

This work was funded by the Wave Energy Scotland Direct Generation Competition and the UK Royal Society IEC-NSFC (223485).

## References

- Alessio, A., Bemporad, A., 2009. A survey on explicit model predictive control. *Nonlinear Model Predictive Control: Towards New Challenging Applications*, 345–369.
- Atyabi, A., Shic, F., Naples, A., 2016. Mixture of autoregressive modeling orders and its implication on single trial eeg classification. *Expert systems with applications* 65, 164–180.
- Banjac, G., Stellato, B., Moehle, N., Goulart, P., Bemporad, A., Boyd, S., 2017. Embedded code generation using the osqp solver, in: 2017 IEEE 56th Annual Conference on Decision and Control (CDC), IEEE. pp. 1906–1911.
- Bank, B., Guddat, J., Klatte, D., Kummer, B., Tammer, K., 1982. *Non-linear parametric optimization*. volume 58. Walter de Gruyter GmbH & Co KG.
- Barstow, S., Mørk, G., Lønseth, L., Mathisen, J.P., 2011. Worldwaves wave energy resource assessments from the deep ocean to the coast. *Journal of Energy and Power Engineering* 5, 730–742.
- Bemporad, A., 2015. A quadratic programming algorithm based on nonnegative least squares with applications to embedded model predictive control. *IEEE Transactions on Automatic Control* 61, 1111–1116.
- Bemporad, A., 2021. Explicit model predictive control, in: *Encyclopedia of systems and control*. Springer. pp. 744–751.
- Clément, A., McCullen, P., Falcão, A., Fiorentino, A., Gardner, F., Hammarlund, K., Lemonis, G., Lewis, T., Nielsen, K., Petroncini, S., et al., 2002. Wave energy in europe: current status and perspectives. *Renewable and sustainable energy reviews* 6, 405–431.
- Drew, B., Plummer, A.R., Sahinkaya, M.N., 2009. A review of wave energy converter technology.
- Evans, M.A., Cannon, M., Kouvaritakis, B., 2014. Robust mpc tower damping for variable speed wind turbines. *IEEE Transactions on Control Systems Technology* 23, 290–296.
- Faedo, N., Olaya, S., Ringwood, J.V., 2017. Optimal control, mpc and mpc-like algorithms for wave energy systems: An overview. *IFAC Journal of Systems and Control* 1, 37–56.
- Faizal, M., Ahmed, M.R., Lee, Y.H., 2014. A design outline for floating point absorber wave energy converters. *Advances in Mechanical Engineering* 6, 846097.
- Falnes, J., Kurniawan, A., 2020. *Ocean waves and oscillating systems: linear interactions including wave-energy extraction*. volume 8. Cambridge university press.
- Fusco, F., Ringwood, J.V., 2012. A simple and effective real-time controller for wave energy converters. *IEEE Transactions on sustainable energy* 4, 21–30.
- Gray, W.S., Verriest, E.I., 2006. Algebraically defined gramians for nonlinear systems, in: *Proceedings of the 45th IEEE Conference on Decision and Control*, IEEE. pp. 3730–3735.
- Hals, J., Falnes, J., Moan, T., 2011. A comparison of selected strategies for adaptive control of wave energy converters .
- Hillis, A., Whitlam, C., Brask, A., Chapman, J., Plummer, A., 2020. Active control for multi-degree-of-freedom wave energy converters with load limiting. *Renewable Energy* 159, 1177–1187.
- Houzhong, Z., Jiasheng, L., Chaochun, Y., Xiaoqiang, S., Yingfeng, C., 2020. Application of explicit model predictive control to a vehicle semi-active suspension system. *Journal of Low Frequency Noise, Vibration and Active Control* 39, 772–786.
- Hredzak, B., Agelidis, V.G., Demetriades, G., 2015. Application of explicit model predictive control to a hybrid battery-ultracapacitor power source. *Journal of Power Sources* 277, 84–94.
- Jariwala, A.M., Dash, S.K., Sahu, U.K., Mohan, H.M., 2025. Performance optimization techniques on point absorber and oscillating water column wave energy converter: A comprehensive review. *IEEE Access* .
- Jiang, H., Lin, J., Song, Y., You, S., Zong, Y., 2016. Explicit model predictive control applications in power systems: an agc study for an isolated industrial system. *IET Generation, Transmission & Distribution* 10, 964–971.
- Jusoh, M.A., Ibrahim, M.Z., Daud, M.Z., Albani, A., Mohd Yusop, Z., 2019. Hydraulic power take-off concepts for wave energy conversion system: A review. *Energies* 12, 4510.
- Khan, N., Kalair, A., Abas, N., Haider, A., 2017. Review of ocean tidal, wave and thermal energy technologies. *Renewable and Sustainable Energy Reviews* 72, 590–604.
- Korde, U.A., Ringwood, J., 2016. *Hydrodynamic control of wave energy devices*. Cambridge University Press.
- Kothare, M.V., Balakrishnan, V., Morari, M., 1996. Robust constrained model predictive control using linear matrix inequalities. *Automatica* 32, 1361–1379.
- Lasheen, A., Saad, M.S., Emara, H.M., Elshafei, A.L., 2017. Continuous-time tube-based explicit model predictive control for collective pitching of wind turbines. *Energy* 118, 1222–1233.
- Li, G., Belmont, M.R., 2014. Model predictive control of sea wave energy converters–part i: A convex approach for the case of a single device. *Renewable Energy* 69, 453–463.
- Li, Q., Murai, M., Kitazawa, D., 2020. Short-time wave force prediction and control strategy for a point-absorber wec. *Ocean Engineering* 218, 108000.
- Moore, B., 1981. Principal component analysis in linear systems: Controllability, observability, and model reduction. *IEEE transactions on automatic control* 26, 17–32.

- Murai, M., Li, Q., Funada, J., 2021. Study on power generation of single point absorber wave energy converters (pa-wecs) and arrays of pa-wecs. *Renewable Energy* 164, 1121–1132.
- Murai, M., Sakamoto, S., 2022. A basic study on the effect of deep learning to determine the control force to maximize the power generation of pa-wec in irregular waves, in: *International Conference on Offshore Mechanics and Arctic Engineering*, American Society of Mechanical Engineers. p. V004T05A015.
- Nian, X., Fu, X., Chu, X., Xiong, H., Wang, H., 2020. Disturbance observer-based distributed sliding mode control of multimotor web-winding systems. *IET Control Theory & Applications* 14, 614–625.
- Patrinos, P., Bemporad, A., 2013. An accelerated dual gradient-projection algorithm for embedded linear model predictive control. *IEEE Transactions on Automatic Control* 59, 18–33.
- Privara, S., Široký, J., Ferkl, L., Cigler, J., 2011. Model predictive control of a building heating system: The first experience. *Energy and Buildings* 43, 564–572.
- Qiu, S., Liu, K., Wang, D., Ye, J., Liang, F., 2019. A comprehensive review of ocean wave energy research and development in china. *Renewable and Sustainable Energy Reviews* 113, 109271.
- Ricker, N.L., 1985. Use of quadratic programming for constrained internal model control. *Industrial & Engineering Chemistry Process Design and Development* 24, 925–936.
- Ringwood, J.V., Bacelli, G., Fusco, F., 2014. Energy-maximizing control of wave-energy converters: The development of control system technology to optimize their operation. *IEEE control systems magazine* 34, 30–55.
- Suman, S.K., Kumar, A., 2021. Linear system of order reduction using a modified balanced truncation method. *Circuits, Systems, and Signal Processing* 40, 2741–2762.
- Wang, H., Wijaya, V.V., Zhang, Y., Zeng, T., Dong, X., 2024. Non-causal control for wave energy conversion based on the double deep q network, in: *2024 UKACC 14th International Conference on Control (CONTROL)*, IEEE. pp. 13–18.
- Wang, Y., Boyd, S., 2009. Fast model predictive control using online optimization. *IEEE Transactions on control systems technology* 18, 267–278.
- Weiss, G., Li, G., Mueller, M., Townley, S., Belmont, M., 2012. Optimal control of wave energy converters using deterministic sea wave prediction, in: *The energy & materials research conference*, Torremolinos, Malaga, Spain.
- Xiao, Y., Ding, F., Zhou, Y., Li, M., Dai, J., 2008. On consistency of recursive least squares identification algorithms for controlled auto-regression models. *Applied Mathematical Modelling* 32, 2207–2215.
- Xu, S., Wang, S., Soares, C.G., 2019. Review of mooring design for floating wave energy converters. *Renewable and Sustainable Energy Reviews* 111, 595–621.
- Yang, S., Chen, H., Ji, Z., Li, H., Xiang, X., 2021. Modelling and analysis of inertia self-tuning phase control strategy for a floating multi-body wave energy converter. *IET Renewable Power Generation* 15, 3126–3137.
- Yu, S., Maier, C., Chen, H., Allgöwer, F., 2013. Tube mpc scheme based on robust control invariant set with application to lipschitz nonlinear systems. *Systems & Control Letters* 62, 194–200.
- Yu, Z., Falnes, J., 1995. State-space modelling of a vertical cylinder in heave. *Applied Ocean Research* 17, 265–275.
- Zhan, S., Li, G., 2018. Linear optimal noncausal control of wave energy converters. *IEEE Transactions on Control Systems Technology* 27, 1526–1536.
- Zhan, S., Li, G., Bailey, C., 2019a. Economic feedback model predictive control of wave energy converters. *IEEE Transactions on Industrial Electronics* 67, 3932–3943.
- Zhan, S., Li, G., Na, J., He, W., 2019b. Feedback noncausal model predictive control of wave energy converters. *Control Engineering Practice* 85, 110–120.
- Zhan, S., Na, J., Li, G., Wang, B., 2018. Adaptive model predictive control of wave energy converters. *IEEE Transactions on Sustainable Energy* 11, 229–238.
- Zhang, J., Lyu, M., Shen, T., Liu, L., Bo, Y., 2017. Sliding mode control for a class of nonlinear multi-agent system with time delay and uncertainties. *IEEE Transactions on Industrial Electronics* 65, 865–875.
- Zhang, Y., Li, G., 2019. Non-causal linear optimal control of wave energy converters with enhanced robustness by sliding mode control. *IEEE Transactions on Sustainable Energy* 11, 2201–2209.
- Zhang, Y., Stansby, P., Li, G., 2020. Non-causal linear optimal control with adaptive sliding mode observer for multi-body wave energy converters. *IEEE Transactions on Sustainable Energy* 12, 568–577.
- Zhang, Y., Zeng, T., Li, G., 2019. Robust excitation force estimation and prediction for wave energy converter m4 based on adaptive sliding-mode observer. *IEEE Transactions on Industrial Informatics* 16, 1163–1171.